THE JOURNAL OF PHYSICAL CHEMISTRY C

Article

pubs.acs.org/JPCC

Catalytic Mechanisms of Sulfur-Doped Graphene as Efficient Oxygen Reduction Reaction Catalysts for Fuel Cells

Lipeng Zhang, Jianbing Niu, Mingtao Li, and Zhenhai Xia*

Department of Materials Science and Engineering, Department of Chemistry, University of North Texas, Denton, Texas 76203, United States

ABSTRACT: Density functional theory (DFT) was applied to study sulfur-doped graphene clusters as oxygen reduction reaction (ORR) cathode catalysts for fuel cells. Several sulfur-doped graphene clusters with/without Stone−Wales defects were investigated and their electronic structures, reaction free energy, transition states, and energy barriers were calculated to predict their catalytic properties. The results show that sulfur atoms could be adsorbed on the graphene surface, substitute carbon atoms at the graphene edges in the form of sulfur/sulfur oxide, or connect two graphene sheets by forming a sulfur cluster ring. These sulfur-doped graphene clusters with sulfur or sulfur oxide locating at graphene edges show electrocatalytic activity for ORR. Catalytic active sites distribute at the zigzag edge or the neighboring carbon atoms of doped sulfur oxide atoms, which possess large spin or charge density. For those being the active catalytic sites, sulfur atoms with the highest charge density take a two-electron transfer pathway while the carbon atoms with high spin or charge density follow a four-electron transfer pathway. It was predicted from the reaction energy barriers that the sulfur-doped graphene could show ORR catalytic properties comparable to platinum. The prediction is consistent with the experimental results on S-doped graphene.

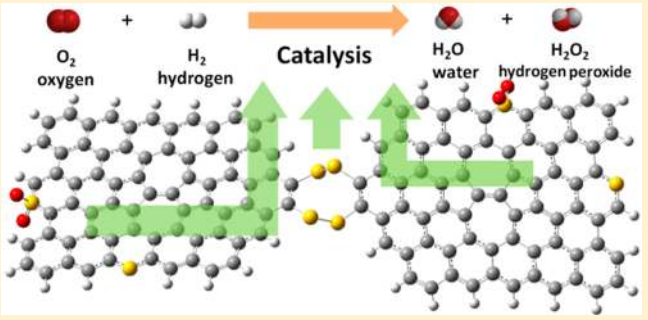

1. INTRODUCTION

High conversion efficiency, high power density, quiet operation, and no pollution are the remarkable advantages of fuel cells for various applications. However, the kinetics of the oxygen reduction reaction (ORR) on cathode is sluggish without catalysts.[1,2] In principle, the ORR can process through direct four-electron transfer pathway, $O_2 + 4H^+ + 4e^- \rightarrow 2H_2O$, or two-electron transfer pathway in which hydrogen peroxide formed, $O_2 + 2H^+ + 2e^- \rightarrow H_2O_2$. The former pathway is expected to occur to achieve high efficiency. Thus, a route to search for an efficient catalyst is to determine if this catalyst facilitates the four-electron pathway. So far, the most effective electrocatalyst for ORRs on cathode is Pt or its alloys, which proceeds through four-electron transfer.[3,4] However, the high cost, limited supply, poor durability, and stability of Pt have hindered the large-scale application of fuel cells. Therefore, the search for new nonprecious metal[5−8] or metal-free[9−12] catalysts with high activity and practical durability has received a great deal of interest.

Graphene, a two-dimensional monolayer structure of sp^2 hybridization carbon, has attracted great attention in a wide range of fields, such as electronics,[13,14] sensors,[15,16] batteries,[17,18] and catalysts,[19] due to its exceptional properties.[20−22] Both theoretical and experimental studies have revealed that doped heteroatoms such as nitrogen and boron can modify their electrical properties and chemical activities.[23] Recently, studies have confirmed that N-doped carbon materials, such as carbon nanotubes (CNTs),[9,24] graphene,[19,25] and mesoporous graphitic arrays,[26] exhibit high electrocatalytic activity and CO tolerance in comparison to conventional platinum catalysts for ORR and are promising candidates for replacing Pt-based catalysts. B-doped[27] and N/B-codoped graphene[28] also show high catalytic property for ORR. The high activity of these doped graphenes (nitrogen, nitrogen/boron) may be attributed to the polarized distribution of spin and charge density[29,30] which are caused by the introduced heteroatoms. More recently, sulfur-doped graphene has been synthesized by using different methods,[12,31,32] which exhibits competitive catalytic activities compared to nitrogen-doped graphene and even better catalytic activities than commercial Pt/C. Experimental results show that the onset potential and the number of transferred electrons per oxygen for S-doped graphene are close to those for the nitrogen-doped graphene.[12,19] The sulfur-doped graphene expands the family of metal-free carbon-based nanomaterials as a new electrocatalyst to replace Pt in fuel cells.

Density functional theory (DFT) is an effective theoretical method to study the electronic property of catalytic materials and ORR pathways. The prominent pathway of ORR in proton exchange membrane (PEM) fuel cell and the kinetics of the proposed nonelectrochemical reactions were studied by using the DFT method.[33] The mechanisms of ORR on carbon-

Received: October 23, 2013
Revised: January 3, 2014
Published: January 29, 2014

   dx.doi.org/10.1021/jp410501u | J. Phys. Chem. C 2014, 118, 3545−3553

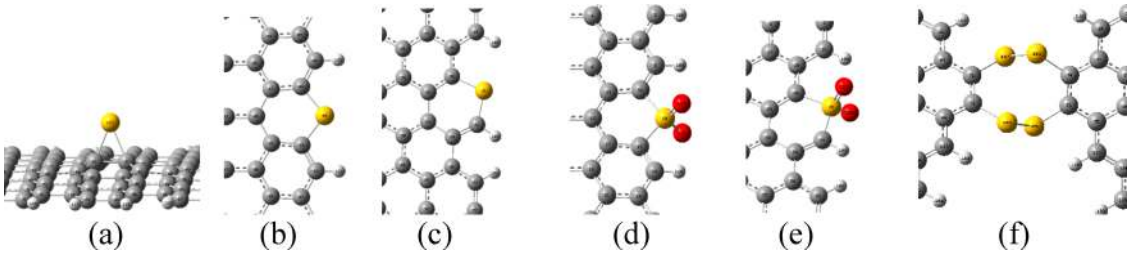

Figure 1. Several possible sulfur-doped graphene clusters: (a) sulfur atoms adsorbed on the surface of the graphene cluster; substituting sulfur atoms at (b) zigzag and (c) armchair edges; SO_2 substituted at (d) zigzag and (e) armchair edges; and (f) sulfur ring cluster connecting two pieces of graphene. The structures of the graphene are shown only partially to highlight the doping structures. Small white, gray, yellow, and red balls represent hydrogen, carbon, sulfur, and oxygen atoms, respectively.

supported Fe-phthalocyanine (FePc/C) and Co-ptthalocyanine (CoPc/C) in alkaline solution were also elucidated.[34] Anderson et al. applied the DFT method on studying the oxygen reduction on graphene, nitrogen-doped graphene, and cobalt−graphene−nitride systems.[35−37] Recently, Zhang et al. using the DFT method studied the ORR mechanisms on the nitrogen-doped graphene[29] effect of the microstructure (the number of dopants and defects) of nitrogen-doped graphene for ORR in acidic environment.[30] They proposed a four-electron ORR pathway on N-doped graphene, and that Stone−Wale defects facilitate the ORR on nitrogen-doped graphene. Furthermore, DFT calculations were also used to study the mechanisms of ORR on N-doped graphene in an alkaline environment by Yu et al.,[38] who took the solvent, surface coverage, and adsorbates into consideration, and obtained the overall energy profile of the ORR pathway. Although the nitrogen/boron-doped graphenes have been studied theoretically,[39−41] little work was done on the sulfur-doped graphene, and their effect on the ORR. Sulfur belongs to the *p*-block of the periodic table, which have unique electronic structures (*p* orbitals in the outermost shell) similar to nitrogen, but with different electronegativities. It is of interest to explore the catalytic mechanism of S-doped graphene. In this work, using DFT calculation, we studied the doping structure of sulfur atoms on the graphene clusters and their catalytic mechanism for ORR in an acidic environment. These sulfur-doped graphene clusters show electrocatalytic activity for ORR, which strongly depends on their doping structures.

2. METHODS

B3LYP hybrid density functional theory (DFT) of Gaussian 09 (Revision A. 02; Gaussian, Inc.: Wallingford, CT, 2009) was employed with a basis set of 6-31G (d,p).[29] Four possible types of sulfur-doped graphene clusters (SGC) were considered, as schematically shown in Figure 1. Type one is sulfur atoms adsorbed on the surface of the graphene cluster ($C_{100}H_{26}S$). Type two represents the sulfur atom substitution at the zigzag or armchair edge of the graphene cluster ($C_{99}H_{25}S$). In Type three, the sulfur atom substitutes the carbon atoms at the graphene edge (zigzag and armchair) in the form of $-C-SO_2-C-$ ($C_{99}H_{25}SO_2$). The last type is two pieces of graphene clusters connected by a sulfur ring ($C_{144}H_{40}S_4$). For comparison, pure graphene ($C_{100}H_{26}$) was also analyzed in this study. These models of sulfur bonding structures are built based on the experimental structure analyses of sulfur-doped graphene.[31,42,43] X-ray photoelectron spectroscopy (XPS) shows all the high-resolution S2p peaks of sulfur-doped graphene could be resolved into three different peaks at binding energies of ∼163.9, 165.1, and 168.9 eV, respectively. The former two peaks were corresponding to $2p_{3/2}$ and $2p_{1/2}$ positions of thiophene-S due to their spin−orbit coupling. The third peak related to some oxidized sulfur. Binding energies around 162.0 eV (S−H) and higher than 165.5 eV were not found. So the sulfur are inferred to be mainly doped at the edges or on the surface of graphene in the form of −C−S−C− or $-C-SO_2-C-$. To reduce the calculation expense and show the effect of sulfur bonding structures on the local electronic properties of graphene at the same time, we model a sheet of graphene with 100 carbon atoms, the edged carbon atoms of which are terminated by hydrogen atoms. These graphene clusters are large enough to study the local effect of doping while having good computational efficiency. In these doped graphene clusters, Stone−Wales defects were also introduced to study defect effects. Stone−Wales defects are one type of important topological defects in sp^2-bonded carbon materials, which could affect the electronic property of graphene. The optimization structures of all these sulfur-doped graphene clusters were calculated by using the DFT. Formation energies of these SGC were calculated as follows: $E_f = E_{S\text{-graphene}} + y\mu_C - (E_{graphene} + x\mu_{S/S\text{-oxide}})$, where $E_{S\text{-graphene}}$ is the energy of SGC, $E_{graphene}$ is the energy of the corresponding graphene cluster, μ_C is the chemical potential of C, and $\mu_{S/S\text{-oxide}}$ is the chemical potential of S_8 or sulfur oxide (SO_2), respectively.

The ORR processes were simulated to explore possible reaction pathways in the presence of SGC. In an acidic environment, a unified mechanism for the first reduction step, which combines Damjanovic's proton participation in the first electron reduction step and Yeager's dissociative chemisorptions of O_2, is summarized as follows as Path I

$$O_2 + H^+ \rightarrow OOH^+ \quad (1)$$

$$OOH^+ + * + e^- \rightarrow *OOH \quad (2)$$

or Path II

$$O_2 + * + e^- \rightarrow *O-O^- \quad (3)$$

$$*O-O^- + H^+ \rightarrow *OOH \quad (4)$$

where the asterisk represents a chemisorption site on the graphene cluster. In Path I, O_2 first reacts with a proton to form OOH^+[30] and then adsorb on active sites of the graphene cluster after the first electron transmission was completed. To examine this reaction path, we set an OOH molecule near the graphene cluster plane at a distance of 1.5−3 Å, and then observed if it adsorbs on the graphene surface. We also set the O_2 molecule near the graphene to check whether it could adsorb at the potential catalytic active sites or not. After the first electron transformation, the succeeding electron transforming was

dx.doi.org/10.1021/jp410501u | J. Phys. Chem. C 2014, 118, 3545−3553

Table 1. Formation Energy (eV) of S-Doped Graphene Clusters

graphene clusters	surface adsorption P 1	surface adsorption P 2	zigzag edge substitution	armchair edge substitution	SO_2- zigzag edge substitution	SO_2- armchair edge substitution	ring clustering
without defect	−1.46	−1.73	0.90	2.02	1.47	2.73	2.70
with defect	−2.60	−2.31	0.89	1.80	1.44	2.37	2.54

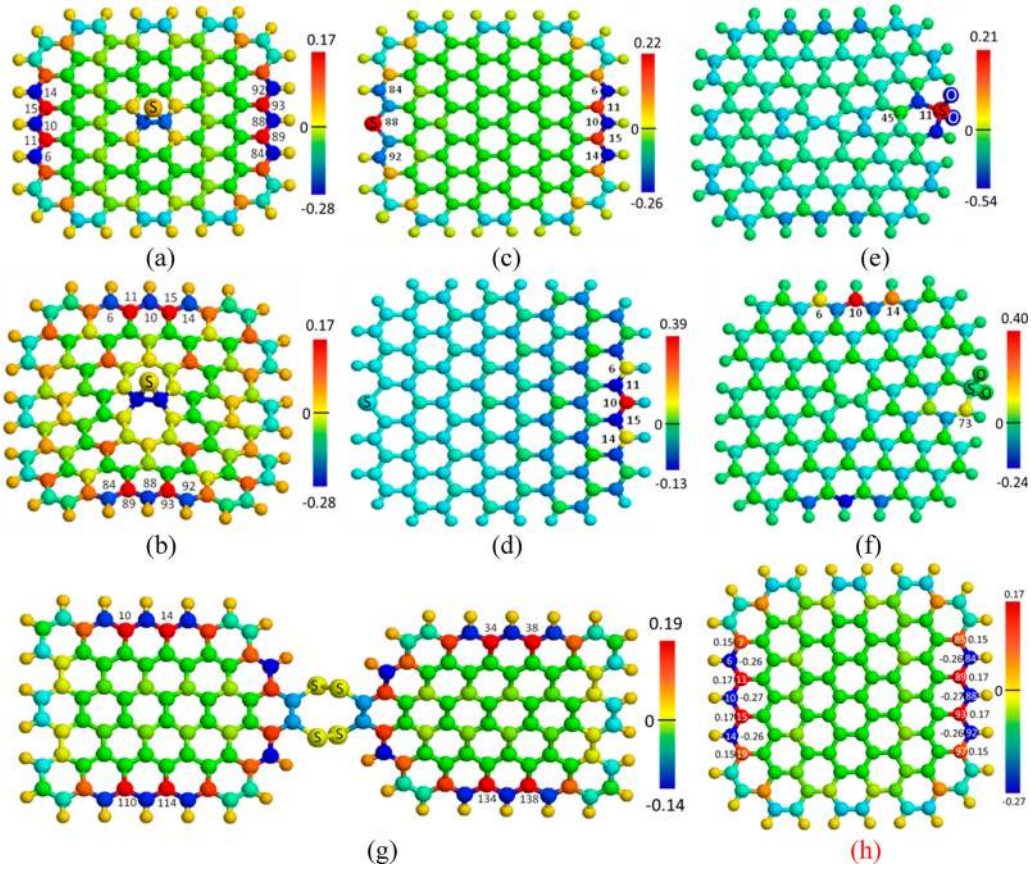

Figure 2. Atomic charge density and spin density distributions on the S-doped and pure graphene clusters. Atomic charge density distribution on S-adsorbed graphene clusters with (a) perfect structure and (b) one Stone−Wales defect; (c) atomic charge density and (d) spin density distributions on perfect graphene cluster with substituting S at the zigzag edge; (e) atomic charge density and (f) spin density on SO_2-doped graphene with a Stone−Wales defect; atomic charge density on (g) sulfur ring cluster connecting two pieces of graphene clusters and (h) pure graphene cluster. The colors of the balls stand for relative values of charge and spin density. The density decreases linearly from positive to negative values in the color order of red, orange, yellow, green, and blue. Sulfur and oxygen atoms are labeled with S and O, respectively. The unlabeled small and large balls represent H and C, respectively.

simulated by adding H atoms in the system. For each step, we obtained the transition state structures and optimized structures, and calculated the reaction energy barrier ΔE_b and reaction free energy ΔG. ΔE_b is defined as the difference between the energy of transition structures (E_T) and initial structures (E_I), $\Delta E_b = E_T - E_I$, and ΔG is the difference between free energies of the final and initial states given by the following expression:[44,45] $\Delta G = \Delta E + \Delta ZPE - T\Delta S$, where ΔE is the reaction energy calculated by the difference of chemical potential between product and reactant molecules adsorbed on the catalyst surface, obtained from DFT calculations of optimization structures, ZPE is the zero point energy, S is the entropy, which are obtained by calculating the frequency of optimization structure, and T is the temperature. For the reaction with negative reaction free energy, it would occur spontaneously.

3. RESULTS AND DISCUSSION

3.1. Doped Graphene Clusters and Formation Energy.

Figure 1 shows four possible sulfur-doping graphene clusters, namely, sulfur chemisorption on surface, S substitution at edge, SO_2 substitution at edge, and sulfur ring clusters, which have been described in detail in the Methods section. The formation energies of these sulfur-doped graphenes were calculated and are listed in Table 1. The formation energies for sulfur adsorbing on the graphene surface (Figure 1a) are negative, but they are positive for sulfur or sulfur oxide substitution at the edges of graphene clusters (Figure 1b−e) and the sulfur ring cluster connecting graphene clusters (Figure1f). Therefore, compared to the sulfur (or sulfur oxide) edge substitution (Figure 1b−e) or sulfur ring cluster connecting graphene (Figure 1f) sulfur adsorption on the graphene surface is energetically favorable. In the presence of Stone−Wales defects on the graphene cluster, the formation energies of sulfur-doped graphene clusters are lower than those of perfect graphene

dx.doi.org/10.1021/jp410501u | J. Phys. Chem. C 2014, 118, 3545−3553

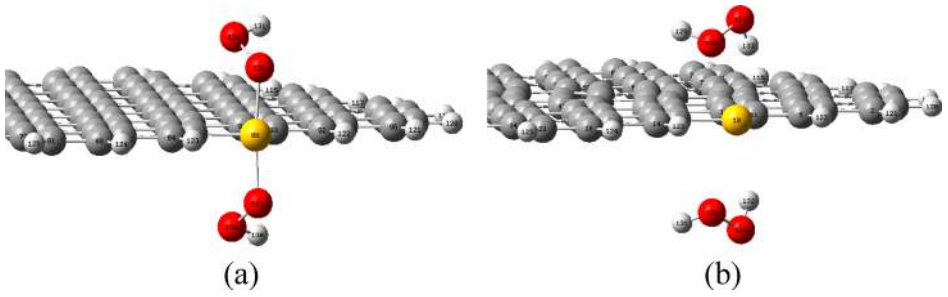

Figure 3. ORR process on the sulfur-doped graphene cluster when the catalytic active site is the sulfur atom: (a) two OOH molecules adsorbed on the sulfur atom and (b) two H_2O_2 molecules formed and departed from the sulfur atom after the introduction of two more H atoms.

clusters. So Stone–Wales defects facilitate sulfur doping on the graphene clusters. This may be attributed to the fact that defects change the local charge distribution and crystal lattice. For the edge substitution, the difference in the formation energy between the perfect and the defective graphene cluster is ~0.36 eV, lower than that of the sulfur (sulfur oxide) adsorbing on the graphene surface or the sulfur ring cluster graphene. Thus, Stone–Wales defects at the center of the graphene cluster have a weak effect on the sulfur edge substitution. For the same graphene cluster, the formation energy of sulfur atoms (sulfur oxide) at the zigzag edge is always lower than that of the armchair one, suggesting that sulfur (sulfur oxide) is preferable to substitute the carbon atoms at the zigzag edge.

3.2. Active Catalytic Sites of the S-Doped Graphene Clusters. We calculated spin and charge densities of each atom of the sulfur-doped graphene clusters and determined possible ORR catalytic active sites on these doped structures on the basis of these spin and charge density distributions. It was shown in our prior work[29,30] that the ORR catalytic active sites are closely related to the charge and spin density distributions. Figure 2 shows the atomic charge and spin density distributions on the sulfur-doped and pure graphene clusters. For the sulfur-adsorbed graphene surface, the sulfur atom does not introduce an extra unpaired electron, therefore, the graphene does not exhibit additional spin density. The charge density, on the other hand, redistributes on the perfect or defective (Stone–Wales defects) S-doped graphene cluster (Figure 2a,b). Specifically, carbon atoms designated with the numbers 11, 15, 89, and 93 at the zigzag edge possess higher positive charge density around 0.17. These carbon atoms may be the catalytic active sites for ORR. To test this hypothesis, we have calculated the adsorption of OOH or O_2 species on these sites by setting them near these potential catalytic sites. The adsorption of OOH or O_2 species is the first step necessary for the graphene to catalyze the ORR. The results show that both OOH and O_2 can adsorb on these atoms located at the zigzag edge of graphene with Stone–Wales defects but cannot on the graphene without Stone–Wales defects. Thus, those S-adsorbed graphene could have catalytic activities depending on the Stone–Wales defects. Here, the defects play an important role in facilitating the ORR. Compared to the perfect graphene cluster, the sulfur-doped graphene surface twisted a little bit when the Stone–Wales defects were introduced, which changed the crystal lattice and local charge distribution on the graphene cluster.

Panels c and d of Figure 2 show the atomic charge and spin density distributions on the graphene cluster with substitutional sulfur atoms located at the zigzag edge, respectively. Similar to those above, the atoms with high charge density are also located at the zigzag edge. Furthermore, spin density is also introduced on the atom at the edge. For example, the edge carbon atoms 11 and 15 possess the highest charge density of 0.19 among the carbon atoms. For spin density, edge atom 10, with the largest value of 0.39, and edge atoms 6 and 14, with the second largest value of 0.27, are found on the graphene. In addition, the sulfur atom (number 88) obsesses a maximum positive charge density of 0.22. Similar spin and charge density distributions can be found on the defective graphene structures with sulfur oxide atom at the armchair edge (Figure 2e,f). Besides, the neighboring carbons at the doped sulfur oxide also have high spin and charge densities. Here, again, the Stone–Wales defects make the sulfur-doped graphene clusters polarized more atoms with higher spin and charge density can be found on the doped graphene cluster with Stone–Wales defects than those on the perfect one, suggesting that the defects could generate more catalytic active sites to ORR. For the sulfur ring cluster connecting two pieces of graphene cluster, these atoms with higher charge density are also at the zigzag edge or neighboring the sulfur atoms on the graphene clusters, but the value is less than 0.19 (Figure 2g). We have tested these atoms with the high charge or spin density and confirmed that all these atoms with charge density larger than 0.20 and spin density larger than 0.15 can adsorbe OOH or O_2 and could be potential active sites for ORR. To demonstrate the effect of the doped sulfur atom, we also calculated the charge density distribution on the pure graphene cluster. As shown in Figure 2h, there is no spin density on the pure graphene cluster, and the maximum value of charge density is 0.17. The overall charge distribution is similar to that on the graphene cluster having sulfur atom chemisorption. OOH or O_2 could not adsorb on any of its carbon atoms with higher charge density. Thus the catalytic capability of the pure graphene is limited.

3.3. ORR Pathway on Sulfur-Doped Graphene. *3.3.1. Two-Electron Transfer Paths.* Once an OOH is adsorbed on the doped graphene surface, the next step of the ORR could be the O–O bond break, which represents four-electron transfer. Otherwise, the ORR is a two-electron transfer. We have examined all the possible active sites selected on the basis of large positive charge density and spin density, and simulated the reaction when a proton is added to the position near adsorbed OOH. We found that the ORR is either four-electron or two-electron transfer depending on the doping structures. In the case of the sulfur atom being the catalytic active site, two OOH species can adsorb on the S atom (Figure 3a). The distance between adsorbed oxygen (OOH) and sulfur atoms decreased to 1.8 Å from the original distance of 3.0 Å after structural optimization. Thus, the S–O covalent bond

dx.doi.org/10.1021/jp410501u | J. Phys. Chem. C 2014, 118, 3545–3553

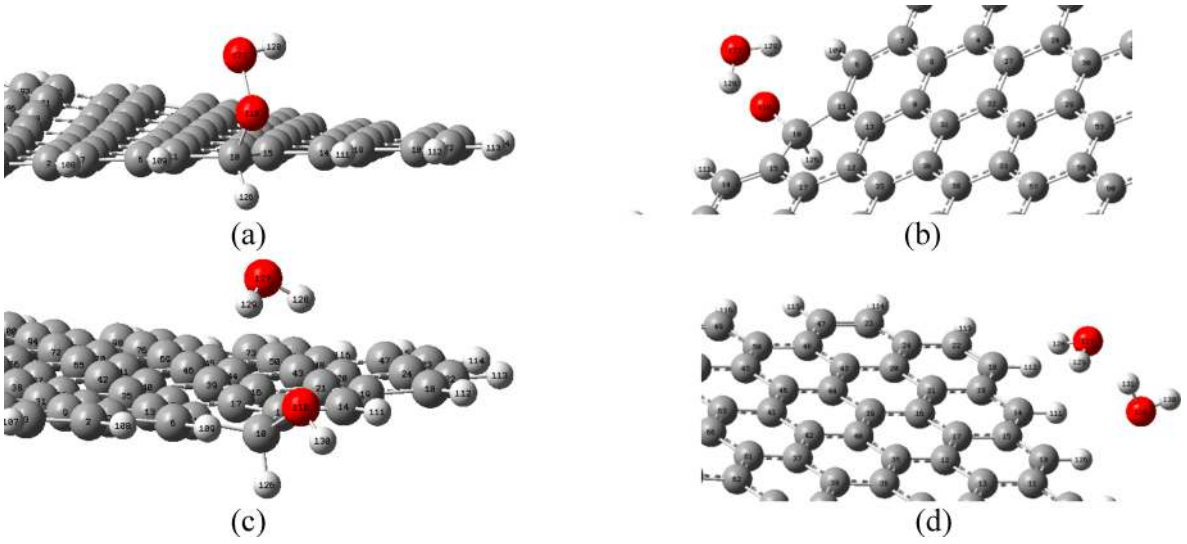

Figure 4. ORR processes on the sulfur-doped graphene cluster where a carbon atom at the zigzag edge acts as the catalytic active site because of the highest spin density on it: (a) OOH adsorbed on the carbon atom, (b) rupture of the O−O bond and formation of the water molecule after an H atom was introduced into the system, (c) formation of an OH after the second H was introduced, and (d) formation of another water molecule after the third H was introduced into the system.

formed and the OOH chemically adsorbed on the S atom. As two more H atoms were set near the oxygen atoms of two OOH species, they adsorbed to the oxygen atoms in OOH molecules that were bonded to the sulfur atom, respectively. The bonds between sulfur and oxygen atoms break in the reaction, resulting in the formation of two H_2O_2 molecules. Finally, H_2O_2 molecules moved away from the graphene surface. The final distance between the H_2O_2 and graphene is 3.5 Å (Figure 3b).

3.3.2. Four-Electron Transfer Paths. For these carbon atoms with large spin or charge density as catalytic active sites, it was found that the four-electron transfer usually occurs. For example, for edge S-doped graphene, OOH was able to adsorb to atom number 10, the carbon with the highest spin density (Figure 4a). When a proton was introduced near the adsorbed OOH, it resulted in rupture of the O−O bond and formation of one water molecule while one oxygen atom still adsorbed on the graphene alone (Figure 4b). As mentioned above, the breakage of the O−O bond is the key step of four-electron transfer, which defines the process being the four-electron transfer pathway. After two protons were successively introduced into the system, as shown in Figure 4c,d, another water molecule formed and departed from the graphene. The finial distance between the two water molecules and graphene is ∼3.4 Å.

The above calculations show that for S-doped graphene those carbons with high charge or spin density facilitate four-electron transfer while the sulfur itself promotes two-electron transfer. As mentioned before, two-electron transfer ORR is inefficient. Although sulfur doping activates carbon atoms as active sites for four-electron transfer ORR, the existence of the sulfur dopants reduces the efficiency of the ORR. However, among these doping structures, the $-SO_2-$ bonding structure (Figure 1d,e) does not catalyze the two-electron transfer reactions while it activates carbon atoms for ORR. We thus suggest that the catalytic efficiency may be improved by introducing $-SO_2-$ bonding structures during the graphene doping process.

3.4. Reaction Free Energy and Energy Barriers.

Reaction free energy ΔG was calculated for each substep of the ORR over sulfur-doped graphene clusters. For the first electron-transfer process, ΔG was determined for two different mechanisms (Paths I and II) since Damjanovic's proton participation reactions and/or Yeager's dissociative mechanism may occur on the same graphene. Values of ΔG for two- and four-electron transfer pathways are listed in Table 2. For the

Table 2. Reaction Free Energy, ΔG (eV), of Two-Electron and Four-Electron Transfer Reaction Processes on Sulfur-Doped Graphene with and without Stone−Wales Defects[a]

sub-reactions			no defects	defects
two-electron transfer pathway		$O_2 + H^+ + e^- \rightarrow$ *OOH	−0.17	−0.15
	path I	$O_2 + H^+ + e^- \rightarrow$ OOH	−1.20	−1.20
		OOH + * → *OOH	1.03	1.05
	path II	O_2 + * → $*O_2$	CF	DA
		$*O-O + H^+ + e^- \rightarrow *O-O-H$		
		$*OOH + H^+ + e^- \rightarrow H_2O_2$	−1.33	−1.36
		$O_2 + 2H^+ + e^- \rightarrow H_2O_2$	−1.50	−1.51
four-electron transfer pathway		$O_2 + H^+ + e^- \rightarrow$ *OOH	−1.21	−1.45
	path I	$O_2 + H^+ + e^- \rightarrow$ OOH	−1.20	−1.20
		OOH + * → *OOH	−0.01	−0.25
	path II	O_2 + * → $*O_2$	−0.58	−0.88
		$*O-O + H^+ + e^- \rightarrow *O-O-H$	−0.63	−0.57
		$*OOH + H^+ + e^- \rightarrow *O + H_2O$	−0.80	−0.83
		$*O + H_2O + H^+ + e^- \rightarrow *OH + H_2O$	−1.38	−1.59
		$*OH + H_2O + H^+ + e^- \rightarrow 2H_2O$	−1.60	−1.03
		$O_2 + 4H^+ + 4e^- \rightarrow 2H_2O$	−4.99	−4.90

[a]No defects and defects stand for these graphene clusters without and with Stone−Wales defects, respectively; the asterisk refers to chemi-adsorption on graphene; CF stands for calculation convergence failure; DA stands for O_2 dis-adsorption on graphene.

dx.doi.org/10.1021/jp410501u | J. Phys. Chem. C 2014, 118, 3545−3553

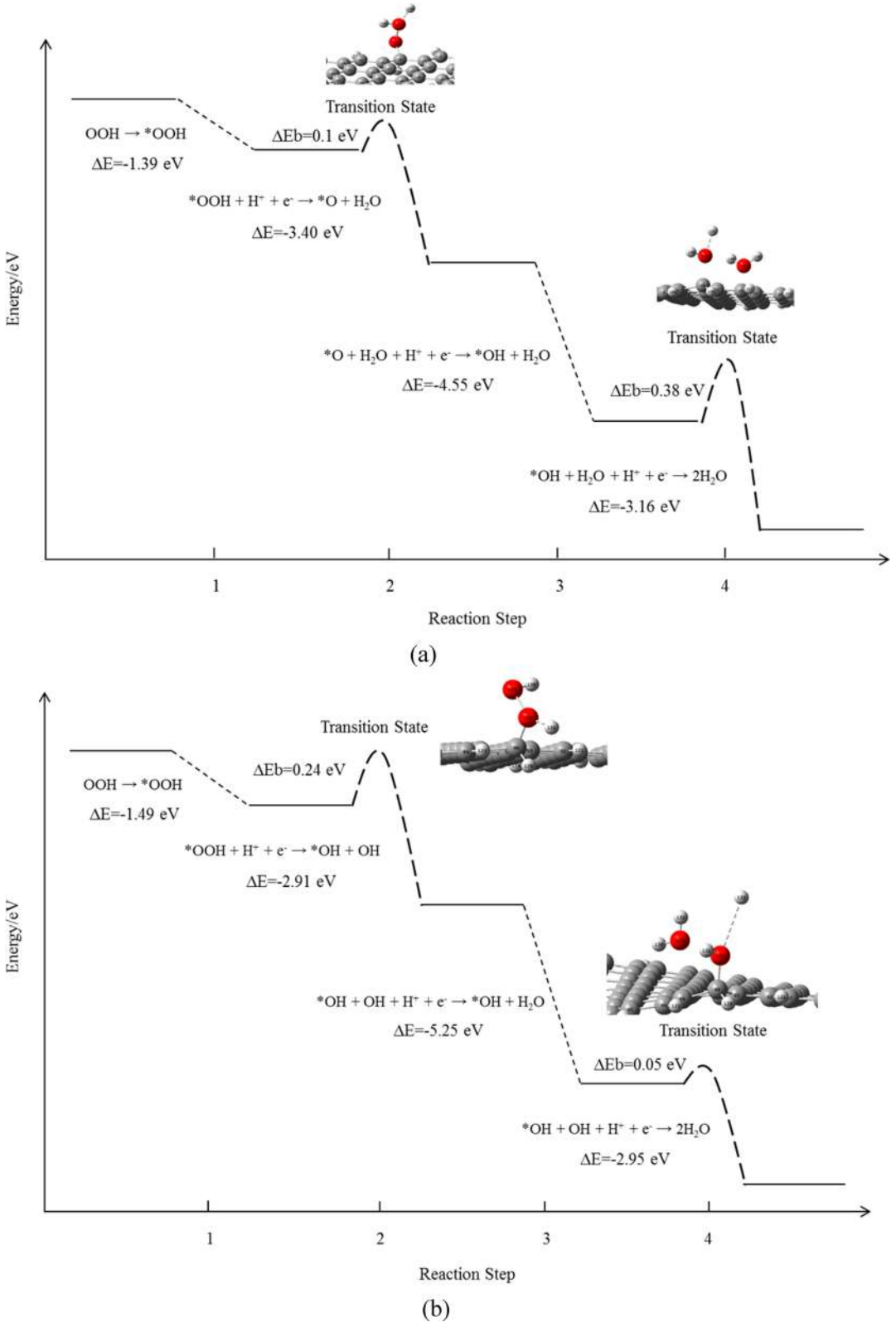

Figure 5. Reaction energy diagram of ORR on (a) sulfur- and (b) sulfur oxide-doped graphene clusters.

first electron transmission of the two-electron transfer ORR on the graphene cluster with sulfur atoms being the catalytic active sites, Damjanovic's proton participation reactions 1 and 2 seem to be energetically unfavorable if these two reactions occur separately because ΔG is negative (−1.20 eV) for reaction 1 but positive (1.03−1.05 eV) for reaction 2. However, these two reactions could occur if one-electron transfer takes place to form OOH in the solvent, followed by the adsorption of the neutral OOH on the graphene. For four-electron transfer which takes place at carbon active sites, reactions 1 and 2 could occur successively as ΔG for them is all negative. For the two-electron transfer ORR, Yeager's dissociation might not occur because O_2

dx.doi.org/10.1021/jp410501u | J. Phys. Chem. C 2014, 118, 3545−3553

could not adsorb on any potential catalytic active sites. For the four-electron transfer, O_2 adsorption and the following proton reactions (reactions 3 and 4) could occur successively, as the values of ΔG are all negative.

After the first electron transfer whether the reactions follow Path I or II, the intermediate products are the same, OOH adsorbed on the graphene. The reaction free energy of all subreactions for two- or four-electron transfer paths is negative for these sulfur-doped graphenes, indicating that the reaction process would be energetically favorable. In our models, the two-electron transfer usually occurs at the S-doped sites, which possesses the highest positive charge density, while the four-electron transfer proceeds mostly on carbon atoms with the high positive spin or charge density. Thus, both sulfur- and sulfur oxide-doped graphene would show high catalytic activities. For the sulfur-adsorbed graphene, the presence of Stone−Wales defects is critical for the graphene to catalyze ORR.

We have compared our calculations with the experimental results for sulfur-doped graphene clusters. For the two-electron transfer reaction, $O_2 + 2H^+ + e^- \rightarrow H_2O_2$, our simulation predicts that the free energies are −1.50 and −1.51 eV for those sulfur-doped graphene clusters without and with Stone−Wales defects, respectively, which are close to the experimental value (ΔG = −1.40 eV) in standard states.[35] For the four-electron transfer pathway on the sulfur-doped graphene cluster without and with defects, overall reaction $O_2 + 4H^+ + 4e^- \rightarrow 2H_2O$, calculated values of ΔG are −4.99 and −4.90 eV, which are also close to the experimental results (ΔG = −4.92 eV) in standard states.[44] Thus, both two- and four-electron transfer processes could simultaneously occur in thermodynamics on these sulfur-doped graphene clusters, and the number of electron transfer could be between 2 and 4. This conclusion is consistent with the experimental results that show the number of transferred electrons ranging from 2.51 to 3.82 for the sulfur-doped graphene.[12]

Although the above reactions over the S-doped graphene clusters are thermodynamically favorable, the kinetics of the ORR catalytic activities is determined by energy barriers ΔE_b of each reaction. It is necessary to determine the transition states and reaction energy barriers of subreactions over the Sulfur-doped graphene cluster. Here taking the reactions on sulfur (shown in Figure 5a) and oxide sulfur (shown in Figure 5b) at the zigzag edge of graphene clusters as examples, we determined the transition states and calculated the reaction energy barriers. For the first reaction step, we found that there is no reaction energy barrier for the OOH molecule adsorbing on the catalytic active sites of the sulfur and oxide sulfur at the zigzag edge of graphene clusters. Since the reaction energies of the first step are −1.39 and −1.49 eV, respectively, for these two doped graphene clusters, the first step is not a key step affecting the reaction kinetics. The transition states in the second step, the O−O bond breakage, are shown in Figure 5. For the S-doped graphene cluster, the transition state is that the *OOH still adsorbs on the active site of the graphene but a proton is close to OOH with a O−H distance of 1.71 Å (inset of Figure 5a). The energy barrier was calculated to be 0.1 eV for the reaction where one water molecule and one adsorbed *O are generated on the graphene. A similar transition structure with a O−H distance of 1.56 Å (inset of Figure 5b) was found for the oxide sulfur-doped graphene. The energy barrier is 0.24 eV for this reaction, much larger than that for the S-doped graphene, but slightly smaller than the simulation value (ΔE_b = 0.27 eV) for the platinum (111) surface in Sha's work.[46] Our results are comparable to the simulation results for nitrogen-doped graphene (ΔE_b = 0.19 eV), and nitrogen-doped carbon nanotube (ΔE_b = 0.30 eV).[47] In the third electron transfer step, there is no energy barrier found for both sulfur- and sulfur oxide-doped graphene clusters, but in the last step, the formation of water molecules, the reaction barriers are 0.38 and 0.05 eV for these sulfur- and sulfur oxide-doped graphenes, respectively. These values are also comparable to that (ΔE_b = 0.21 eV) for the same reaction over platinum (111).[46] Overall, the doping with $-SO_2-$ bonding structures seems better in terms of the energy barriers and the number of electron transfer. Since the energy barriers are comparable for the same reactions over these materials, the sulfur-doped graphene may show ORR catalytic properties similar to platinum, N-doped graphene, and carbon nanotubes. This prediction has been proved to be consistent with the experimental results on S-doped graphene.[12,32]

4. CONCLUSION

Four types of sulfur-doping structures, surface S-adsorbed, edge S-substituted, edge SO_2-substituted, and sulfur-ring connecting graphene clusters, were proposed based on the experimental results. The formation energy, electronic structures, as well as ORR catalytic activities were calculated via DFT methods. Among these doping structures, surface sulfur adsorption is the most stable structure in terms of formation energy. The active catalytic sites on these S-doped graphene clusters are those carbon atoms located at the zigzag edges or close to the SO_2 doping structure, which possess high positive charge density or spin density. Both two-electron and four-electron transfers can occur simultaneously over the S-doped graphene cluster. Two-electron transfer pathways proceed on the substitutional sulfur atom being the catalytic active sites with high charge density while four-electron transfer takes place on the carbon atoms with high positive spin or charge density. The Stone−Wales defects facilitate the formation of surface S-adsorption on graphene as well as the catalytic activities of sulfur-doped graphene, especially for those with sulfur adsorbing on the surface. The results for transition states and reaction energy barriers of ORR subreactions reveal that the sulfur-doped graphene clusters can show competitively catalytic properties compared with platinum, nitrogen-doped carbon nanotube, and graphene.

AUTHOR INFORMATION

Corresponding Author

*E-mail: zhenhai.xia@unt.edu. Tel: 940-369-5805. Fax: 940-565-4824.

Notes

The authors declare no competing financial interest.

ACKNOWLEDGMENTS

The authors acknowledge the support from AFOSR MURI (FA9550-12-1-0037) and the National Science Foundation (IIP-1343270 and CMMI-1212259).

REFERENCES

(1) Xiong, W.; Du, F.; Liu, Y.; Perez, A.; Supp, M.; Ramakrishnan, T. S.; Dai, L. M.; Jiang, L. 3-D Carbon Nanotube Structures Used as High Performance Catalyst for Oxygen Reduction Reaction. *J. Am. Chem. Soc.* **2010**, *132*, 15839−15841.

(2) Snyder, J.; Fujita, T.; Chen, M. W.; Eelebancher, J. Oxygen Reduction in Nanoporous Metal-Ionic Liquid Composite Electrocatalysts. *Nat. Mater.* **2010**, *9*, 904−907.
(3) Wang, C.; Daimon, H.; Onodera, T.; Kode, T.; Sun, S. H. A General Approach to the Size- and Shape-Controlled Synthesis of Platinum Nanoparticles and Their Catalytic Reduction of Oxygen. *Angew. Chem., Int. Ed.* **2008**, *47*, 3588−3591.
(4) Lim, B.; Jiang, M. J. P.; Cho, E. C.; Tao, J.; Lu, X. M.; Zhu, Y. M.; Xia, Y. N. Pd-Pt Bimetallic Nanodendrites with High Activity for Oxygen Reduction. *Science* **2009**, *324*, 1302−1305.
(5) Zhang, L.; Zhang, J.; Wilkinson, D. P.; Wang, H. Progress in Preparation of Non-noble Electrocatalysts for PEM Fuel Cell Reactions. *J. Power Sources* **2006**, *156*, 171−182.
(6) Wu, G.; More, K. L.; Johnston, C. M.; Zelenay, P. High-Performance Electrocatalysts for Oxygen Reduction Derived from Polyaniline, Iron, and Cobalt. *Science* **2011**, *332*, 443−447.
(7) Lefevre, M.; Proietti, E.; Jaouen, F.; Dodelet, J. P. Iron-Based Catalysts with Improved Oxygen Reduction Activity in Polymer Electrolyte Fuel Cells. *Science* **2009**, *324*, 71−74.
(8) Byon, H. R.; Suntivich, J.; Shao-Horn, Y. Graphene-Based Non-Noble-Metal Catalysts for Oxygen Reduction Reaction in Acid. *Chem. Mater.* **2011**, *23*, 3421−3428.
(9) Gong, K. P.; Du, F.; Xia, Z. H.; Durstock, M.; Dai, L. M. Nitrogen-Doped Carbon Nanotube Arrays with High Electrocatalytic Activity for Oxygen Reduction. *Science* **2009**, *323*, 760−764.
(10) Wang, S.; Yu, D.; Dai, L. Polyelectrolyte Functionalized Carbon Nanotubes as Efficient Metal-free Electrocatalysts for Oxygen Reduction. *J. Am. Chem. Soc.* **2011**, *133*, 5182−5185.
(11) Yang, L.; Jiang, S.; Zhao, Y.; Zhu, L.; Chen, S.; Wang, X.; Wu, Q.; Ma, J.; Ma, Y.; Hu, Z. Boron-Doped Carbon Nanotubes as Metal-Free Electrocatalysts for the Oxygen Reduction Reaction. *Angew. Chem., Int. Ed.* **2011**, *50*, 7132−7135.
(12) Yang, Z.; Yao, Z.; Li, G.; Fang, G.; Nie, H.; Liu, Z.; Zhou, X.; Chen, X. a.; Huang, S. Sulfur-Doped Graphene as an Efficient Metal-free Cathode Catalyst for Oxygen Reduction. *ACS Nano* **2012**, *6*, 205−211.
(13) Li, X. L.; Zhang, G. Y.; Bai, X. D.; Sun, X. M.; Wang, X. R.; Wang, E.; Dai, H. J. Highly Conducting Graphene Sheets and Langmuir Blodgett Films. *Nat. Nanotechnol.* **2008**, *3*, 538−542.
(14) Lee, C.; Wei, X.; Kysar, J. W.; Hone, J. Measurement of the Elastic Properties and Intrinsic Strength of Monolayer Graphene. *Science* **2008**, *321*, 385−389.
(15) Patil, A. J.; Vickery, J. L.; Scott, T. B.; Mann, S. Aqueous Stabilization and Self-Assembly of Graphene Sheets into Layered Bionanocomposites Using DNA. *Adv. Mater.* **2009**, *21*, 3159−3164.
(16) Lu, C. H.; Yang, H. H.; Zhu, C. L.; Chen, X.; Chen, G. N. A Graphene Platform for Sensing Biomolecules. *Angew. Chem., Int. Ed.* **2009**, *48*, 4785−4787.
(17) Wu, Z. S.; Ren, W. C.; Xu, L.; Li, F.; Cheng, H. M. Doped Graphene Sheets as Anode Materials with Superhigh Rate and Large Capacity for Lithium Ion Batteries. *ACS Nano* **2011**, *5*, 5463−5471.
(18) Yoo, E.; Kim, J.; Hosono, E.; Zhou, H.; Kudo, T.; Honma, I. Enhanced Cyclic Performance and Lithium Storage Capacity of SnO_2/Graphene Nanoporous Electrodes with Three-Dimensionally Delaminated Flexible Structure. *Nano Lett.* **2008**, *8*, 2277−2282.
(19) Qu, L. T.; Liu, Y.; Baek, J. B.; Dai, L. M. Nitrogen-Doped Graphene as Efficient Metal-free Electrocatalyst for Oxygen Reduction in Fuel Cells. *ACS Nano* **2010**, *4*, 1321−1326.
(20) Novoselov, K. S.; Jiang, Z.; Zhang, Y.; Morozov, S. V.; Stormer, H. L.; Zeitler, U.; Maan, J. C.; Boebinger, G. S.; Kim, P.; Geim, A. K. Room-Temperature Quantum Hall Effect in Graphene. *Science* **2007**, *315*, 1379.
(21) Loh, K. P.; Bao, Q. L.; Ang, P. K.; Yang, J. X. The Chemistry of Graphene. *J. Mater. Chem.* **2010**, *20*, 2277−2289.
(22) Lee, C.; Wei, X. D.; Kysar, J. W.; Hone, J. Measurement of the Elastic Properties and Intrinsic Strength of Monolayer Graphene. *Science* **2008**, *321*, 385−388.
(23) Liu, H. T.; Liu, Y. Q.; Zhu, D. Chemical Doping of Graphene. *J. Mater. Chem.* **2011**, *21*, 3335−3345.
(24) Yu, S. S.; Zhang, Q.; Dai, L. M. Highly Efficient Metal-free Growth of Nitrogen-Doped Single-Walled Carbon Nanotubes on Plasma-Etched Substrates for Oxygen Reduction. *J. Am. Chem. Soc.* **2010**, *132*, 15127−15129.
(25) Sheng, Z. H.; Tao, L.; Chen, J. J.; Bao, W. J.; Wang, F. B.; Xia, X. H. Catalyst-free Synthesis of Nitrogen-Doped Graphene via Thermal Annealing Graphite Oxide with Melamine and Its Excellent Electrocatalysis. *ACS Nano* **2011**, *5*, 4350−4358.
(26) Liu, R. L.; Wu, D. Q.; Feng, X. L.; Mullen, K. Nitrogen-Doped Ordered Mesoporous Graphitic Arrays with High Electrocatalytic Activity for Oxygen Reduction. *Angew. Chem., Int. Ed.* **2010**, *49*, 2565−2569.
(27) Sheng, Z.; Gao, H.; Bao, W.; Wang, F.; Xia, X. Synthesis of Boron Doped Graphene for Oxygen Reduction Reaction in Fuel Cells. *J. Mater. Chem.* **2012**, *22*, 390−395.
(28) Wang, S.; Zhang, L.; Xia, Z.; Roy, A.; Chang, D.; Baek, J.; Dai, L. BCN graphene as efficient metal-free electrocatalyst for the Oxygen Reduction Reaction. *Angew. Chem., Int. Ed.* **2012**, *51*, 1−5.
(29) Zhang, L.; Xia, Z. Mechanisms of Oxygen Reduction Reaction on Nitrogen-doped Graphene for Fuel Cell. *J. Phys. Chem. C* **2011**, *115*, 11170−11176.
(30) Zhang, L.; Niu, J.; Dai, L.; Xia, Z. Effect of Microstructure of Nitrogen-doped Graphene on Oxygen Reduction Reaction Activity in Fuel Cell. *Langmuir* **2012**, *28*, 7542−7550.
(31) Yang, S.; Zhi, L.; Tang, K.; Feng, X.; Maier, J.; Müllen, K. Efficient Synthesis of Heteroatom (N or S)-Doped Graphene Based on Ultrathin Graphene Oxide-porous Silica Sheets for Oxygen Reduction Reactions. *Adv. Funct. Mater.* **2012**, *22*, 3634−3640.
(32) Jeon, I.; Zhang, S.; Zhang, L.; Choi, H.; Seo, J.; Xia, Z.; Dai, L.; Baek, J. Edge-Selectively Sulfurized Graphene Nanoplatelets as Efficient Metal-Free Electrocatalysts for Oxygen Reduction Reaction: The Electron Spin Effect. *Adv. Mater.* **2013**, *25*, 6138−6145.
(33) Stephen, W.; Abhishek, D.; Masoud, A.; Heinz, P. Mechanism of Molecular Oxygen Reduction at the Cathode of a PEM Fuel Cell: Non-Electrochemical Reactions on Catalytic Pt Particles. *J. Phys. Chem. C* **2008**, *112*, 8464−8475.
(34) Chen, R. R.; Li, H. X.; Chu, D.; Wang, G. F. Unraveling Oxygen Reduction Mechanisms on Carbon-Supported Fe-Phthalocyanine and Co-Phthalocyanine Catalysts in Alkaline Solutions. *J. Phys. Chem. C* **2009**, *113*, 20689−20697.
(35) Reyimjan, A.; Sidik; Alfred, B. A. O_2 Reduction on Graphite and Nitrogen-Doped Graphite: Experiment and Theory. *J. Phys. Chem. B* **2006**, *110*, 1787−1793.
(36) Ellen, V.; Alfred, B. A. Theoretical Predictions Concerning Oxygen Reduction on Nitrided Graphite Edges and a Cobalt Center Bonded to Them. *J. Phys. Chem. C* **2007**, *111*, 9330−9336.
(37) Kurak, K. A.; Anderson, A. B. Nitrogen-Treated Graphite and Oxygen Electroreduction on Pyridinic Edge Sites. *J. Phys. Chem. C* **2009**, *113*, 6730−6734.
(38) Yu, L.; Pan, X.; Cao, X.; Hu, P.; Bao, X. Oxygen Reduction Reaction Mechanism on Nitrogen-doped Graphene: A Density Functional Theory Study. *J. Catal.* **2011**, *282*, 183−190.
(39) Kim, J. S.; Borisenko, K. B.; Nicolosi, V.; Kirkland, A. I. Controlled Radiation Damage and Edge Structures in Boron Nitride Membranes. *ACS Nano* **2011**, *5*, 3977−3986.
(40) Zhao, L.; He, R.; Gim, K.; Schiros, T.; Kim, K.; Zhou, H.; Gutiérrez, C.; Chockalingam, S. P.; Arguello, C.; Pálová, L.; Nordlund, D.; et al. Visualizing Individual Nitrogen Dopants in Monolayer Graphene. *Science* **2011**, *333*, 999−1003.
(41) Feng, Y.; Li, F.; Hu, Z.; Luo, X.; Zhang, L.; Zhou, X.; Wang, H.; Xu, J.; Wang, E. Tuning the Catalytic Property of Nitrogen-doped Graphene for Cathode Oxygen Reduction Reaction. *Phys. Rev. B* **2012**, *85*, 155454.
(42) Wu, Y.; Fang, S.; Jiang, Y.; Holze, R. Effects of Doped Sulfur on Electrochemical Performance of Carbon Anode. *J. Power Sources* **2002**, *108*, 245−245.
(43) Gao, H.; Liu, Z.; Song, L.; Guo, W.; Gao, W.; Ci, L.; Rao, A.; Quan, W.; Vajtai, R.; Ajayan, P. M. Synthesis of S-doped Graphene by Liquid Precursor. *Nanotechnology* **2012**, *23*, 275605.

(44) Nørskov, J. K.; Rossmeisl, J.; Logadottir, A.; Lindqvist, L. Origin of the Overpotential for Oxygen Reduction at a Fuel-Cell Cathode. *J. Phys. Chem. B* **2004**, *108*, 17886−17892.
(45) Ochtershi, J. W. *Thermochemistry in Gaussian*; Gaussian, Inc.: Wallingford, CT, 2000.
(46) Sha, Y.; Yu, T.; Liu, Y.; Merinov, B.; Goddard, W., III Theoretical Study of Solvent Effects on the Platinum-Catalyzed Oxygen Reduction Reaction. *J. Phys. Chem. Lett.* **2010**, *1*, 856−861.
(47) Ni, S.; Li, Z.; Yang, J. Oxygen Molecule Dissociation on Carbon Nanostructures with Different Types of Nitrogen Doing. *Nanoscale* **2012**, *4*, 1184−1189.